Specific epitopes form extensive hydrogen-bonding networks to ensure efficient antibody binding of SARS-CoV-2: Implications for advanced antibody design

Daojiong Wang [a,1], Yushu Ge [a,*,1], Bin Zhong [a], Dan Liu [a,b,*]

[a] Hefei National Laboratory for Physical Sciences at Microscale, the CAS Key Laboratory of Innate Immunity and Chronic Disease, School of Basic Medical Sciences, Division of Life Sciences and Medicine, University of Science and Technology of China, Hefei 230027, China
[b] The First Affiliated Hospital of University of Science and Technology of China, Hefei 230001, China

ARTICLE INFO

ABSTRACT

Neutralizing antibody targeting to the SARS-CoV-2 could provide powerful therapies. A neutralizing antibody CC12.1 which was found in SARS-CoV-2 patient samples provides potential protection from disease. The aim of molecular dynamics simulations is to identify key epitopes that are crucial to the antibody binding of SARS-CoV-2 spike glycoprotein receptor binding domain (RBD) to promote the development of superior antibodies. Binding modes of the antibody were investigated and compared with RBD bound receptor ACE2. Key epitopes were revealed and a distal motif of RBD (residue numbers 473–488) was demonstrated by analyzing dynamic trajectories. Compared to the receptor ACE2, conformation of RBD could be better stabilized through additional interaction of antibody with the distal motif of RBD, which was further found driven by electrostatic complementarity. By further analysis of the extensive hydrogen-bonding networks, residues D405, K417, Y421, Y453, L455, R457, Y473, A475, N487, G502, Y505 of RBD, which mainly interacted with CDR H3/L3 and two conserved motifs SNY, SGGS, were identified as key epitopes. Higher binding free energy calculated after point mutations on key residues confirms the crucial role for the specific binding. Subsequently, mutations of V_H V98E and V_L G68D in CC12.1, which could significantly enhance the binding affinity of the antibody, were also proposed. The results indicate the key epitopes for antibody binding and give explanations for failure of neutralization antibody caused by specific residues mutations on structural basis. Simulations of two point mutations on antibody provide feasible information for advanced antibody design.

© 2021 The Authors. Published by Elsevier B.V. on behalf of Research Network of Computational and Structural Biotechnology. This is an open access article under the CC BY-NC-ND license (http://creativecommons.org/licenses/by-nc-nd/4.0/).

1. Introduction

The novel severe acute respiratory syndrome coronavirus 2 (SARS-CoV-2), which shares around 77.2% amino acid identify with SARS-CoV [1], have caused much more serious world pandemic [2,3]. More than one hundred million individuals worldwide were infected, and approximately 2,460,000 death cases were reported by 22 Feb 2021 [4]. Up to now, there are still few specific antiviral drugs towards to SARS-CoV-2 show the definite effective treatment benefits in clinical trials [5–8]. Suffice it to say, seeking information used for developing effective therapy against SARS-CoV-2 has become more urgency than ever before. One of the most efficient therapies is using antibody to neutralize virus infectivity [9], and effective antibodies and vaccines are urgently needed [10,11]. Vaccination induces humoral and cellular immune response in immunized individuals and the homologous virus will be neutralized or cleared by neutralizing antibodies (Abs) or specific T cells respectively when it enters an immunized body [12]. Over 200 vaccines are developed, including recombinant protein subunit vaccines, nucleic acid vaccines, viral vector vaccines, inactivated viruses, and live attenuated vaccines [13]. ChAdOx1 nCoV-19 vaccine, one of the vaccines which entered the phase III clinical trials, shows significant vaccine efficacy of 70.4% after two doses and protection of 64.1% after at least one standard dose, against symptomatic disease [14]. Spike glycoprotein (S) of SARS-CoV-2, which was used for most of COVID-19 vaccines, is capable of activating

* Corresponding authors at: Hefei National Laboratory for Physical Sciences at Microscale, the CAS Key Laboratory of Innate Immunity and Chronic Disease, School of Basic Medical Sciences, Division of Life Sciences and Medicine, University of Science and Technology of China, Hefei 230027, China (Y. Ge); The First Affiliated Hospital of University of Science and Technology of China, Hefei 230001, China (D. Liu).
E-mail addresses: geyushu@ustc.edu.cn (Y. Ge), dliu919@ustc.edu.cn (D. Liu).
[1] These authors contribute equally to this work.

the immune system through its antigenic parts and the receptor binding domain (RBD) of spike glycoprotein directly interacts with human receptor ACE2 [15,16]. Whether from patients' serum or synthesis, the neutralizing efficiency of the antibody mainly depends on the binding affinity with the spike glycoprotein RBD of SARS-CoV-2 [17]. Just like SARS-CoV, RBD-binding antibody prevents the recognition by the angiotensin converting enzyme 2 (ACE2) [18], which takes responsible to the fusion mechanism for cellular entry of the virus [19–22]. Despite of high similarity of the sequences and overall structures between the RBD of SARS-CoV-2 and SARS-CoV [23], amino acid mutations cause distinct protein–protein interaction for SARS-CoV-2, which finally lead to various features from molecular to clinical level. First, enhanced receptor binding of SARS-CoV-2 has been determined with more than 10-fold greater binding constant compared to SARS-CoV [24]. Further study showed how networks of hydrogen-bonding and hydrophobic interactions contribute to the enhanced receptor binding [25]. Subsequently, many SARS-CoV directed antibodies, such as S230, m396 and 80R show no cross-reactivity to SARS-CoV-2 [24,26]. Recently separated antibodies responding to SARS-CoV-2 RBD, such as CC12.1 and CC12.3, couldn't neutralize SARS-CoV neither [18]. What mutations contribute to key epitopes causing specific antibody responding? How the potential mutations influence the receptor binding as well as the neutralization efficiency of the antibody? All these questions remain to be answered. In addition, as an RNA virus, the genome of SARS-CoV-2 mutates easily which results in reduced sensitivity to neutralizing antibodies [27,28]. Without the information about key epitopes for antibody binding, it is frustrated to develop vaccines that can induce protective and durable immunity. Clarify the structural mechanism for specific neutralizing antibody would help understand failure neutralization caused by virus mutation, as well as provide essential information for advancing antibody design.

IGHV3-53 gene is the most frequently used IGHV gene for targeting the RBD, and the crystal structures of several encoded antibodies, including CC12.1 as the best, were revealed recently [29]. In this work, we performed and analyzed the molecular dynamics (MD) simulations of the binary complexes of SARS-CoV-2 RBD with the IGHV3-53 encoded antibody and the receptor ACE2. The complex of SARS-CoV RBD with ACE2 was also simulated in parallel for comparison. The simulations represented epitopes distribution of SARS-CoV-2 RBD, especially the critical role of the distal motif of RBD for antibody binding. Key epitopes involved in hydrogen-bonding and salt bridge interactions are identified. Point mutations including V_H V98E and V_L G68D of CC12.1 were explored and proposed for advanced antibody design.

2. Results and discussion

2.1. Conformation of SARS-CoV-2 RBD was stabilized through efficient binding of a distal motif by antibody

Both CC12.1 and ACE2 bind with SARS-CoV-2 RBD through almost the same recognition region. On the structural basis, the competition on the binding surface determines the neutralization efficiency of antibodies. Crystal structure of complex of SARS-CoV-2 RBD and CC12.1 (PDB ID: 6XC2) indicates apparent different contact region around the distal motif of RBD (residue numbers 473–488) compared with ACE2 bound complex (Fig. 1A). CC12.1 forms additional binding with the distal motif while similar contact is absent for ACE2 bound with SARS-CoV-2, as well as for ACE2 bound with SARS-CoV RBD. Analyzing of the trajectories of molecular dynamics simulations lasting for 200 ns of binary complexes of SARS-CoV-2 RBD with CC12.1 and ACE2 indicates that, the superior of almost double fold area on binding surface maintains (Fig. 1B). RMSD values of RBDs and receptor in different systems were calculated and plotted for the whole 200 ns simulation time, which reflected the stability of binary complexes (Fig. 1C and Fig. S1). CC12.1 bound RBD show the highest stability with the lowest RMSD values, followed by ACE2 bound RBD. To take an insight for conformation stabilizing of SARS-CoV-2 RBD, the distributions of residue flexibility in apo, ACE2 bound and CC12.1 bound form were investigated by calculation of RMSF values, respectively. The maximum change of RMSF values occurs in the region of residue numbers 473–488, which is consistent with the distal motif mentioned before (Fig. 1D). Average RMSF value of the region reduced from 5.45 to 2.49 by ACE2 binding, and as low as 1.11 by CC12.1 binding. In the apo form or ACE2 bound form of SARS-CoV RBD, the corresponding region of distal motif also saw the maximum change of RMSF values (Fig. S2). It is reported that SARS CoV-2 invades host cells via CD147 except for ACE2 [30]. The binding mode between human CD147 and SARS-CoV-2 RBD was predicted by docking and the binding region of CD147 is different from ACE2 and CC12.1 with small overlap (Fig. S3). The result indicates that it is possible for SARS-CoV-2 RBD to bind CC12.1 and CD147 both at the same time although CC12.1 may be only binding to SARS-CoV-2 RBD partially.

In summary, comparison of SARS-CoV-2 RBD with CC12.1 and ACE2 binding modes indicates significant larger interface formed with CC12.1 than ACE2. Consistent with the significant structural difference between SARS-CoV-2 and SARS-CoV RBDs in crystal structures [31], the binding on the loop in the distal end of RBD, which was referred as the distal motif (residue numbers 473–488), was found as the most significant difference. It is reported that YQAGSTPCN (residue numbers 473–481) is one of the SARS-CoV-2 spike protein multi-epitopic regions which inspires us to focus on the distal motif next [16].

2.2. Efficient antibody binding of the distal motif was driven by electrostatic complementarity

To better understand the contribution of the enhanced binding interface with the distal motif, sequence BLAST of SARS-CoV-2 RBD as well as human SARS-CoV RBD and some other bat SARS-like coronaviruses was conducted (Fig. S4). It is notable that the motif barely shows any homology with only 4 out of 15 residues sharing conservation with any other coronaviruses that could bind the human ACE2 receptor [32] (Fig. 2A). Thus, enhanced binding with this motif might be the important reason for failure of neutralization of previous SARS-CoV antibodies and the specificity of antibodies for SARS-CoV-2. Considering the sequence differences of the motif among these coronaviruses, it could be speculated that the distal motif wasn't important for ACE2 binding. Furthermore, any mutations of the motif might weaken the binding affinity of current SARS-CoV-2 antibodies with few influences on the binding with receptor ACE2. The consequences will be explored and presented more sufficient in the following sections. Five out of six CDRs of CC12.1 antibody are involved in the binding with RBD (Fig. 2B). For SARS-CoV-2 RBD, residues including Arg403, Lys417, Phe456, Arg457, Tyr473, Ala475, Ser477 and Glu493 were involved and exhibited important roles since these residues mutated in SARS-CoV (Fig. 2A). Computation and mapping of the electrostatic potential of the contact interface indicate obvious complementarity for the corresponding contact area (Fig. 2C). The protruding negative electrostatic potential surface formed by the distal motif enables itself embedded in the positive electrostatic groove formed by CDR H1 of CC12.1. Both contact areas of CC12.1 and ACE2 bind with SARS-CoV-2 RBD are almost the same. However, the distal motif is exposed when ACE2 bound with. It could be assumed that the electrostatic complementary drives the initiate binding of the RBD with CC12.1.
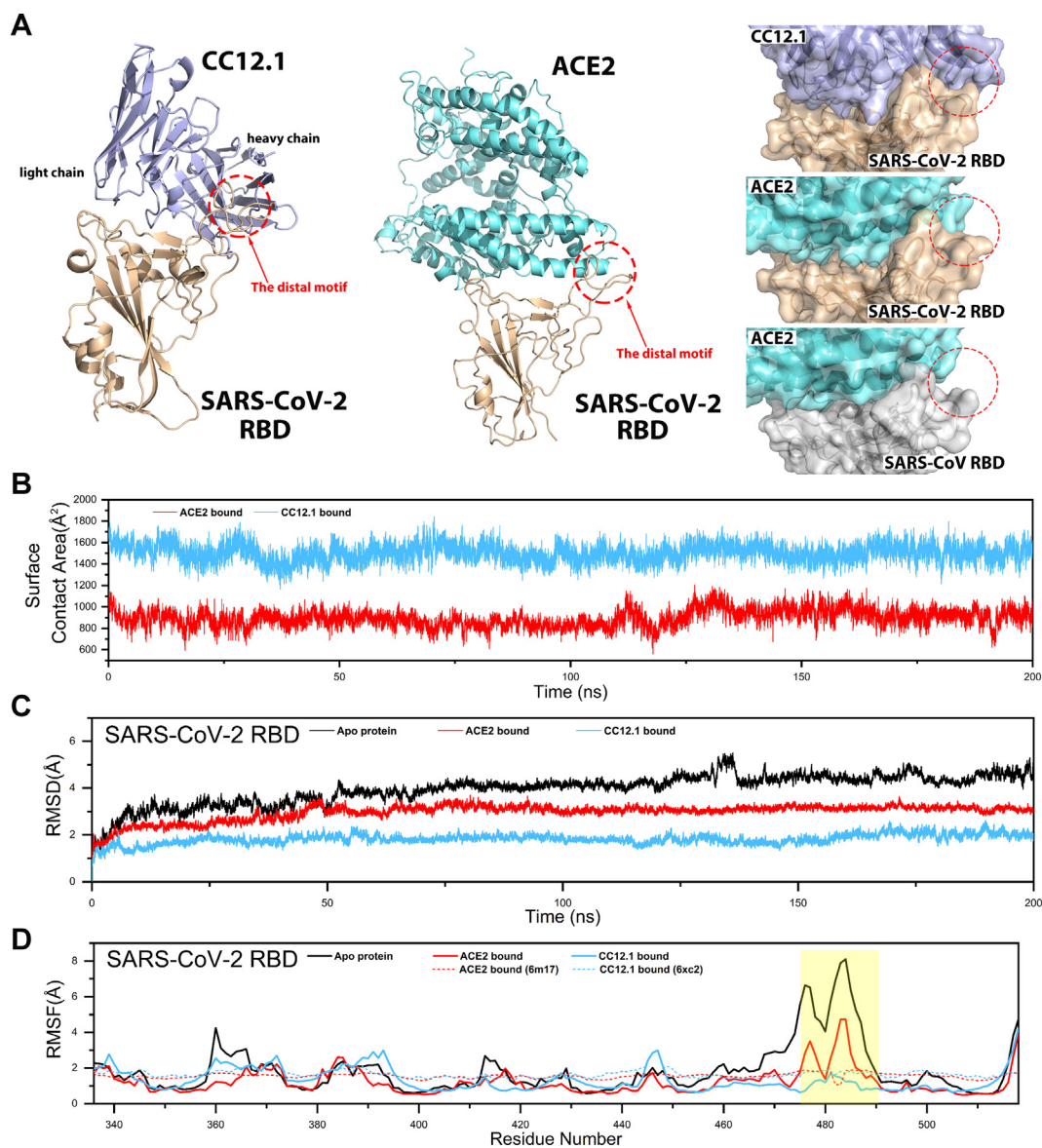
Fig. 1. Crystal structures and the overall view of molecular dynamics simulations results of two complexes. (A) Crystal structures of two complexes used for molecular dynamics simulations, and comparison of interfaces for SARS-CoV-2 RBD binding with ACE2 and antibody as well as SARS-CoV RBD binding with ACE2. Proteins were displayed in cartoon and colored in light blue, wheat and aquamarine for CC12.1 antibody, SARS-CoV-2 RBD and human ACE2 respectively. The distal motif is indicated with red dotted circle (Left). The interfaces of all complexes are displayed in surface view (Right). (B) Computed surface contact area between SARS-CoV-2 RBD and ACE2/CC12.1 during the 200 ns MD simulations. (C) RMSD plotting of SARS-CoV-2 RBD in apo, ACE2 bound and CC12.1 bound forms for 200 ns simulations. (D) RMSF plotting of SARS-CoV-2 RBD in apo, ACE2 bound and CC12.1 bound forms for 200 ns simulations, as well as the value calculated according to b-factors of the corresponding crystal structures (PDB ID: 6M17 and PDB ID: 6XC2). (For interpretation of the references to colour in this figure legend, the reader is referred to the web version of this article.)

2.3. Hydrogen-bonding network plays a central role in antibody binding of the distal motif

In apo protein of SARS-CoV-2 RBD, disulfide bond formed between Cys480 and Cys488 helps to stabilize the distal motif loop [23]. The disulfide bond also remains stable with ACE2 or CC12.1 antibody bound. The distal motif of SARS-CoV-2 RBD anchors in the groove formed between CDR H1 and H3 of antibody. Hydrogen-bonding network formed mainly by three residue pairs was analyzed during the whole 200 ns simulations (Fig. 3A). Hydrogen bonds formed between Y473 and V_H S31, A475 and V_H N32, N487 and V_H R94 dominate the network with the occurrence of 98.23, 99.89 and 99.79%, respectively. For RBD bound with ACE2, three hydrogen bonds in crystal structure could not form stable network during 200 ns simulation. Due to the high flexibility, the

hydrogen bonds formed between G476 and Q24, N487 and Y83 maintain only 31.14% and 35.09% of the whole simulation. A475 and Q24 formed hydrogen bond for only 50 ns and separated ever since (Fig. 3B and Table S1). Each of the three residues, Y473, A475 and N487, could form stable hydrogen-bonding interaction with antibody which was located near Cys480 and Cys488. With the stable disulfide bond formed between Cys480 and Cys488, the three hydrogen bonds provide forces of different orientations to stabilize the binding complex. As for the distal motif with ACE2 bound, only stable disulfide bond couldn't avoid the flexible conformation change. The hydrogen-bonding network stabilizes the conformation of distal motif to a great extent.

It is notable that eight residues in distal motif have been found mutated in SARS-CoV-2 genomes from 3333 samples of the GISAID database [33]. The most frequently mutated residue in distal motif
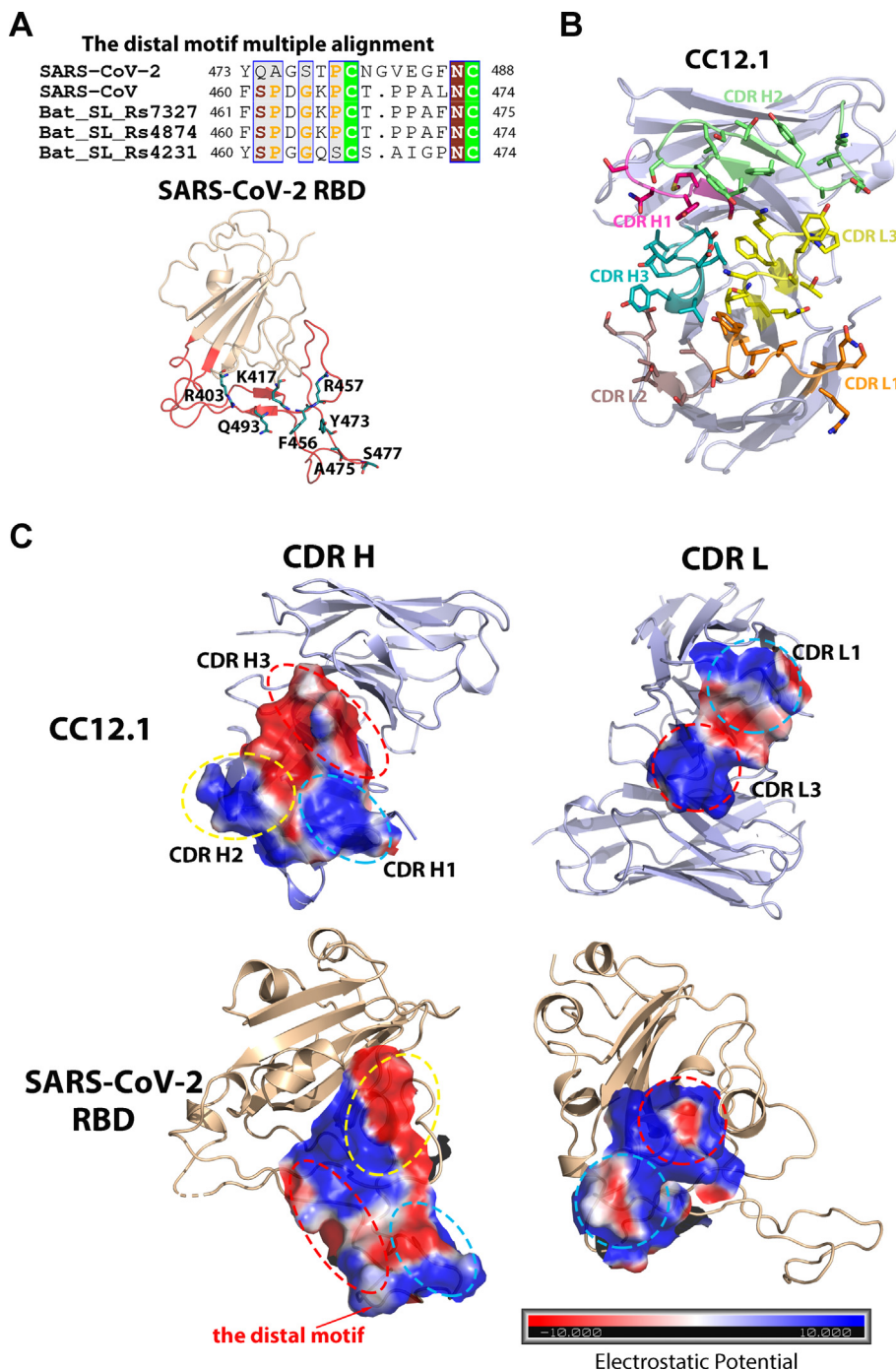
Fig. 2. Crystal structures and computed electrostatic potentials of CC12.1 and the SARS-CoV-2 RBD. (A) Sequence alignment of the distal motif for SARS-CoV-2 and SARS-CoV from human and some other bat SARS-like coronaviruses (Top). Crystal structure of SARS-CoV-2 RBD (Bottom). The receptor binding motif (RBM) located in the interface is labeled in red, and the key residues in RBDs are labeled and shown in sticks. (B) Crystal structure of CC12.1. Protein is displayed in cartoon. The complementarity-determining regions (CDR) are displayed in sticks with individual colors. (C) Computed electrostatic potential distribution of CC12.1 antibody and SARS-CoV-2 RBD. CDRs and its corresponding contact area were circled in dashed line with the same colors. (For interpretation of the references to colour in this figure legend, the reader is referred to the web version of this article.)

is S477, which is first sampled since Jun 2020. (Fig. S5). Sporadic samples have been observed for the other seven mutations, mostly after July 2020. One out of 3333 genomes has the Y473 or T478 or N481 or G482 mutated, four genomes have the V483 mutated, five genomes have the F486 mutated and eight genomes have the E484 mutated. Despite the fact that only sporadic mutations have been found for these residues, the potential impact of these mutations should not be ignored considering the huge and increasing infected population.

2.4. Heavy chain mutation V_H V98E for advanced antibody design and specific epitopes identified for antibody binding

Extensive hydrogen bonds were found between RBD and heavy chain of CDRs. RBD forms four hydrogen bonds with CDR H1, including L455-V_H Y33, Y473-V_H S31, A475-V_H N32, S477-V_H G26 (Fig. 4A). All four hydrogen-bonds show high stability with occurrence of 99.96%, 98.23%, 99.89%, 86.10% during the 200 ns simulation, respectively (Table S1). With CDR H2, R457 and Y421 of RBD
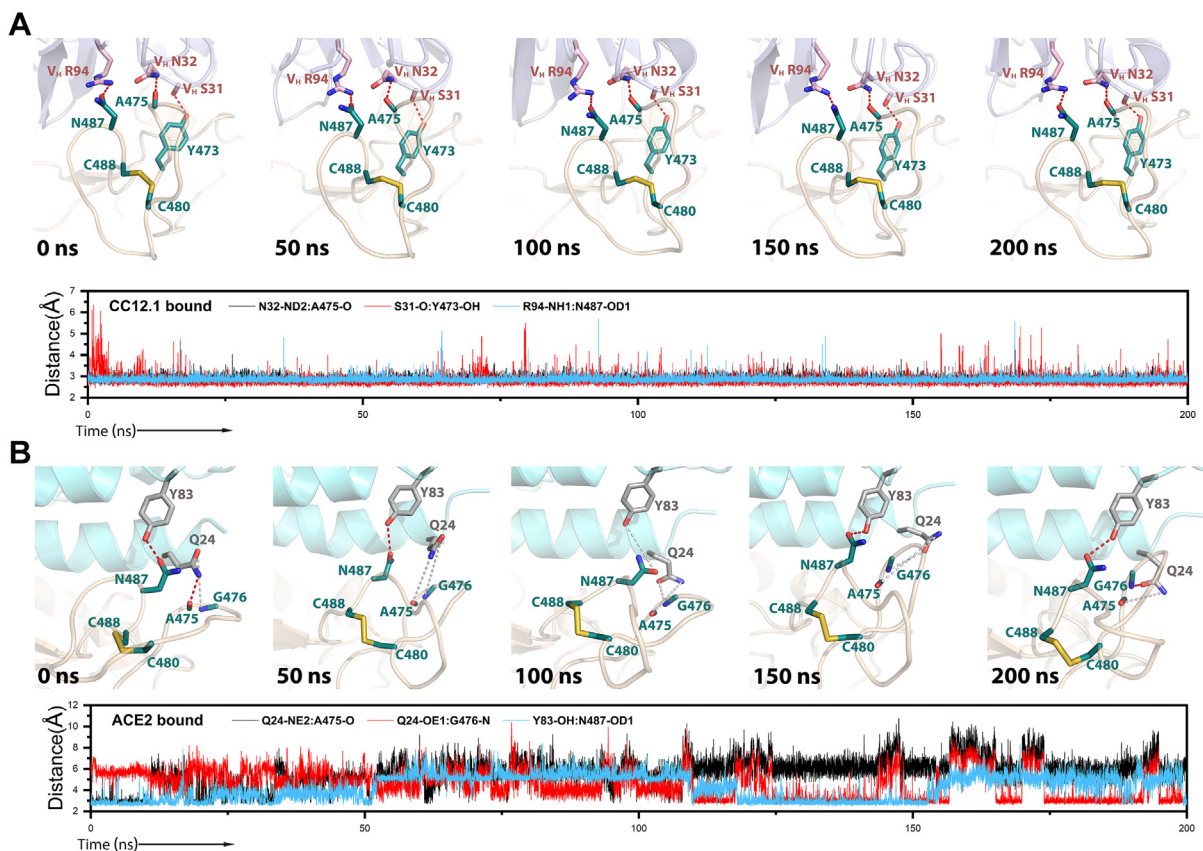
Fig. 3. Snapshots of the distal motif binding with CC12.1 (A) and ACE2 (B) at 0, 50, 100, 150, 200 ns (top panels). Distances between acceptor and donor of each hydrogen bond were plotted at the bottom. Protein is shown as cartoon. Residues involved in hydrogen-bonding are showed as sticks without hydrogen atoms for clarity. Existing hydrogen bonds are shown in red dash lines, dissociated hydrogen bonds are in gray lines. (For interpretation of the references to colour in this figure legend, the reader is referred to the web version of this article.)

form hydrogen bonds with V_H S53 and V_H G54 during 94.44% and 97.25% time of whole simulation, respectively. Meanwhile, V_H S56 could form hydrogen bonds either with D420 or T415 alternatively. The occurrence of two alternate bonding could occupy 92.70% of simulation time which indicates that V_H S56 could form stable interaction with SARS-CoV-2 RBD. Hydrogen bond between V_H S56-D420 was also reported in the previous study [29] (Fig. 4B). At CDR H3, Stable hydrogen-bonding interactions were observed for Y453-V_H D97 and N487-V_H R94 with 96.11% and 99.79% occurrence, respectively. Another hydrogen bond with lower occurrence of 60.76% between Q493 and V_H Y99 was also observed. K417 forms a salt bridge with V_H D97 with the occurrence as high as 73.69% (Fig. 4A and Table S1). In addition, hydrophobic interactions formed between V_H L96 of CC12.1 and F456, Y489 of the RBD were also found to be helpful for efficient binding. Considering the stable hydrogen bonding networks, SNY and SGGS are identified as two motifs that are crucial for antibody binding. The residues in SARS-CoV-2 RBD that interact with SNY and SGGS motifs are predicted as T-cell and B-cell epitopes [34]. Some of these residues, such as D420 and N487, are responsible for antibody-escape mutations which implicates the importance of these two motifs for efficient antibody binding [35]. In view of the conservation of two motifs among other IGHV3-53 encoded antibodies [29], it could be assumed that these two motifs might also be critical for other IGHV3-53 encoded antibodies binding with the SARS-CoV-2 RBD.

Similar interactions between SARS-CoV-2 RBD and ACE2 were investigated to explore the potential mutations for advanced antibody design. Interactions at the same region of RBD for ACE2

bound were found to be much weaker or even absent (Fig. 4A and C). Few hydrogen bonds and salt bridges were found with ACE2 bound. However, two hydrogen bonds formed by G476 (RBD) and Q24 (ACE2), Q493 (RBD) and K31 (ACE2) were observed with occurrence as high as 31.14% and 91.99%, respectively (Table S1). The very stable hydrogen-bonding interaction formed between K31 of ACE2 and Q493 of SARS-CoV-2 RBD is consistent with previous studies [31,36,37]. Due to the lack of the similar interactions for RBD with CC12.1, it could be speculated that mutations mimic the ACE2 binding might improve the antibody binding affinity. Analyzing of interactions of CC12.1 with G476 of RBD indicates alternative hydrogen-bonding with the adjacent residue S477 instead. The intramolecular salt bridge between K31 and D35 of ACE2 was illustrated in previous studies, as well as in our simulation [25,38]. The salt bridge keeps the side chain of K31 toward to the side chain of Q493, which is beneficial for hydrogen-bonding. In CC12.1, none of the similar salt bridge has been observed due to the lack of active amino-group nearby V_H Y99 (Fig. S6). It could be speculated that adding hydrogen bond acceptor atom might lead to similar orientation of side chain of K31 as in ACE2 bound system and binding affinity with the SARS-CoV-2 RBD of antibody could be enhanced through constructing similar interaction. However, the loop conformation of CDRs make the side chains orientations of V_H D97 and V_H Y99 opposite to avoid the potential conformation bump. Mutating V_H Y99 to any other residues couldn't help with the salt bridge interaction forming with V_H D99 or hydrogen-bonding interaction forming with Q493 of SARS-CoV-2 RBD. Considering steric hindrance in this region, single
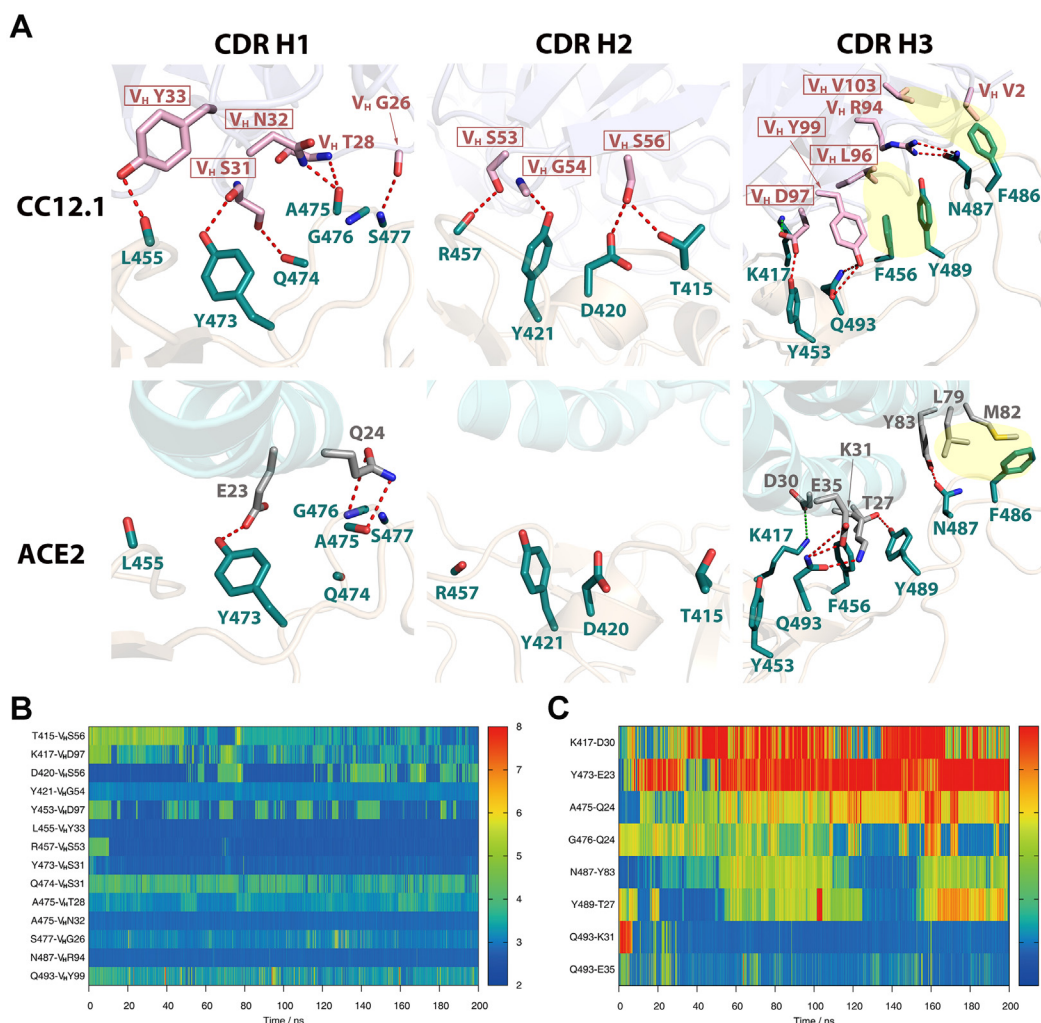
Fig. 4. Represented interactions between SARS-CoV-2 RBD and CDRs of heavy chain as well as ACE2. (A) The RBD, CC12.1, and ACE2 structures are displayed in cartoon and colored in wheat, light blue and aquamarine respectively. Key residues of the RBD, CC12.1, ACE2 are shown as sticks with carbon atoms colored in deep teal, pink, gray, respectively. Hydrogen bonds and salt bridges are displayed in red and green dash lines, respectively. Hydrophobic interactions are shaded in yellow background. The residues belong to CC12.1 CDRs are labeled with rectangular box. Distances between each pair of residues forming hydrogen bond and salt bridge in CC12.1 bound complex (B) and ACE2 bound complex (C) during the 200 ns simulations. (For interpretation of the references to colour in this figure legend, the reader is referred to the web version of this article.)

mutation from V_H V98 to Glu has been established and simulated for 5 ns (Fig. S7A). Q493 forms hydrogen bonds with V_H E98 and V_H L96 successfully, with occurrence as high as 95.00% and 97.00%, respectively. Reduction of −21.36 ± 0.98 kcal/mol for Gibbs binding free energy indicates that the binding affinity with RBD was enhanced significantly (Table 1). The great reduction of binding free energy may not only be caused by the stabilized interaction between Q493 of the RBD and CC12.1, but also the improvement of electrostatic complementarity on proteins interface. The binding mode of CC12.1 with V_H V98E mutation on SARS-CoV-2 RBD was predicted by docking to further validate our results (Fig. S8A). Q493 formed hydrogen bonds with V_H E98 just as we expected. Some stable interactions didn't form after the antibody mutation, probably because docking can't reflect the dynamics properties of proteins and the result is related to the initial structures to a great extent.

In short, residues K417, Y421, Y453, L455, R457, Y473, A475 and N487 of RBD were identified as key epitopes for antibody recognition. Two conserved motifs, SNY and SGGS, are identified for efficient antibody binding. Mutation from V_H V98 to E could significantly improve the binding affinity of antibody.

Table 1
Computed relative binding free energy after point mutation in the SARS-CoV-2 RBD-CC12.1 antibody complex.

Mutation (SARS-CoV-2 RBD-CC12.1 complex)	ΔΔG (kcal/mol)
CC12.1 antibody mutation	
V_H V98 → E	−21.36 ± 0.98
V_L G68 → D	−4.09 ± 1.19
SARS-CoV-2 RBD mutation	
K417 → V	7.41 ± 0.94
Y473 → F	1.06 ± 1.09
A475 → P	5.26 ± 0.99
S477 → G	−2.92 ± 0.98

2.5. Light chain mutation V_L G68D for advanced antibody design and specific epitopes identified for antibody binding

Compared to heavy chain of antibody, fewer hydrogen bonds were found with light chain. All efficient hydrogen bonds were formed with CDR L1 and L3. At CDR L1, V_L G28 and G502, V_L Y32 and G496 form hydrogen bonds with occurrence of 99.78% and 84.06%, respectively (Fig. 5A and Table S1). V_L S30 could form
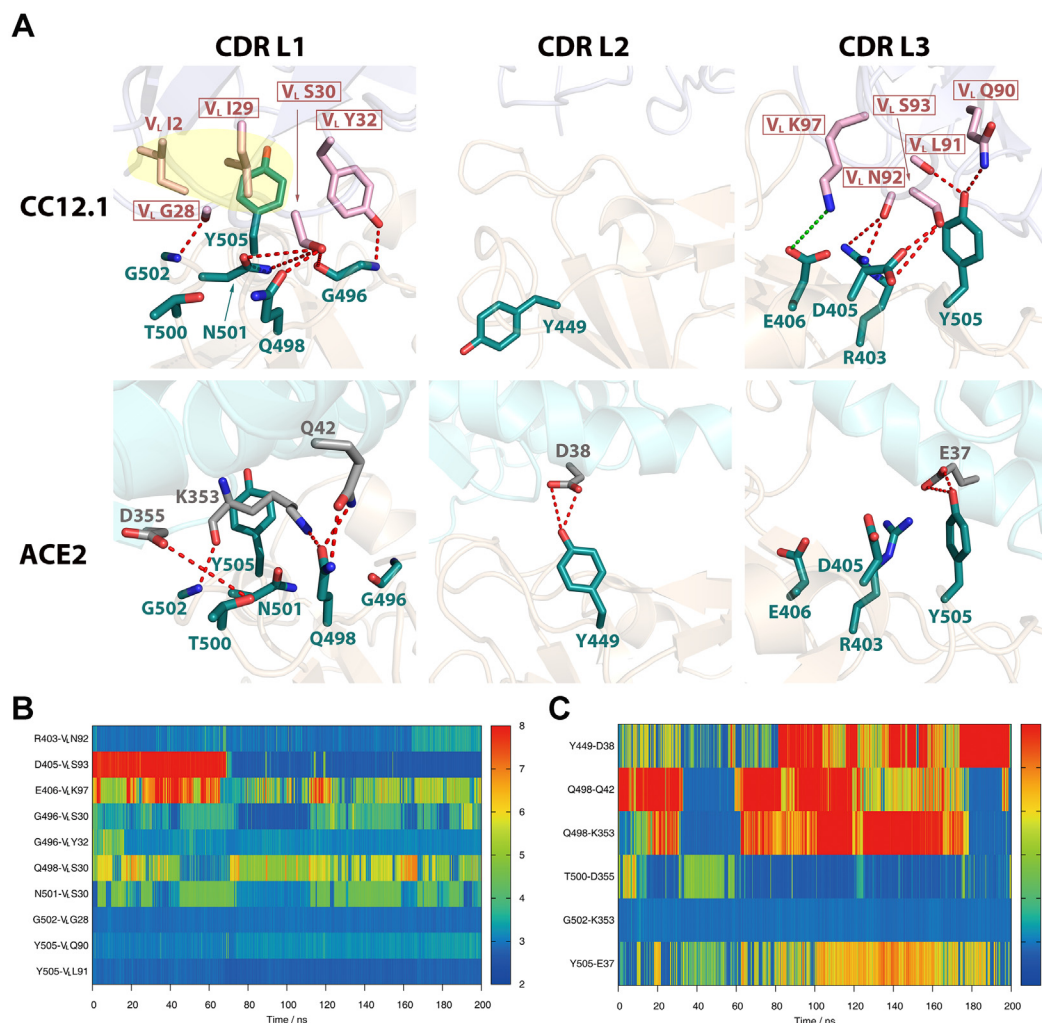
Fig. 5. Represented interactions between SARS-CoV-2 RBD and CDRs of light chain as well as ACE2. (A) The RBD, CC12.1, and ACE2 structures are displayed in cartoon and colored in wheat, light blue and aquamarine respectively. Key residues of the RBD, CC12.1, ACE2 are shown as sticks with carbon atoms colored in deep teal, pink, gray, respectively. Hydrogen bonds and salt bridges are displayed in red and green dash lines, respectively. Hydrophobic interactions are shaded in yellow background. The residues belong to CC12.1 CDRs are labeled with rectangular box. Distances between each pair of residues forming hydrogen bond and salt bridge in CC12.1 bound complex (B) and ACE2 bound complex (C) during the 200 ns simulations. (For interpretation of the references to colour in this figure legend, the reader is referred to the web version of this article.)

hydrogen bond with N501, G496 or Q498 alternatively with total occurrence of 73.63%. At CDR L3, side chain of V_L S93 turns over from outward to inward to RBD gradually along with the simulation and maintains a stable hydrogen bond with D405 after 70 ns (Fig. 5A and B), despite the distance between the corresponding acceptor and donor heavy atoms of hydrogen bond is 8.07 Å in crystal structure. Considering that V_L S93 is also conserved in some IGHV3-53 encoded antibodies [29], V_L S93 may also be another important residue in CDR L for this type of antibodies. Another two efficient hydrogen bonds were found on Y505 with V_L Q90 and V_L L91 at the same time with 86.61% and 99.74% occurrence, respectively (Fig. 5A and Table S1). R403 and V_L N92 form another hydrogen bond and maintain 86.80% of simulation time. In addition, V_L K97 forms an unstable salt bridge with E406 with only 23.02% occurrence and a very stable hydrophobic center was also found among V_L I2, V_L I29 of CC12.1 and Y505 of RBD.

With ACE2 bound, none of interactions were found on R403, D405, G496 and N501 of RBD (Fig. 5A and C). Another fluctuant hydrogen bond between E37 of ACE2 and Y505 of RBD was found with occurrence of 25.33%. Efficient hydrogen-bonding was found on G502 with K353 during 99.61% of simulation, which was

perfectly mimicked by V_L G28 of CC12.1. Another two less stable hydrogen bonds were also found between Q498 and Q42/K353 of ACE2 with only occurrence of 24.36% and 29.26%, respectively. No interactions were observed between RBD and CDR L2 of CC12.1, however, at the corresponding region of ACE2, Y449 of RBD forms a hydrogen bond with D38 of ACE2, although the occurrence is only 20.19%. In CC12.1, the preference of forming intramolecular hydrogen bonds results in the difference of side chain orientation of Y449 between these two complexes. Instead of bonding with G502 or N501 of RBD, D355 of ACE2 forms stable interaction with T500 which is absent in RBD-CC12.1 complex. Corresponding residues of CC12.1 with potential interaction with T500 of RBD were examined to obtain similar efficient interaction. The lowest distance of 4.61 Å was measured between T500 and V_L G68 heavy atoms in crystal structure which is far beyond the effective range to form a stable interaction. Mutation from V_L G68 to D not only provides hydrogen acceptor atoms but also shortens the distance into the effective range. After the 5 ns simulation of mutated complex which was quite stable (Fig. S7A), the binding free energy was calculated. The OG1 atom of T500 forms a hydrogen bond with OD1/OD2 atom of V_L D68 (mutated) alternatively

during the whole 5 ns simulation, which means the V_L G68 → D mutation is helpful in forming efficient interaction with T500 of RBD. Reduction of −4.09 ± 1.19 kcal/mol (Table 1) of the binding free energy indicates the increase of the binding affinity as expected. CC12.1 with V_L G68D mutation was also docked on SARS-CoV-2 RBD (Fig. S8B). The interactions formed between G502/Y505 and mutated CC12.1 were the same as the wild type. As we expected, the OG1 atom of T500 forms a hydrogen bond with OD1 atom of V_L D68.

Overall, these residues, D405, G502 and Y505, which involved in interactions with high occurrence with CC12.1, were identified as key epitopes. The mutation from V_L G68 to D was proposed as a strategy for improving the antibody efficiency. It is noticeable that RBD may be not the only region where the immune-dominant epitopes located in [34,39]. The immuno-dominant epitopes for T-cell and B-cell have been predicted by various immunoinformatics methods, and other predicted immune-dominant epitopes in spike glycoprotein of SARS-CoV-2 indicate potential protective antibodies sites [40].

2.6. CC12.1 binds to SARS-CoV-2 but not SARS-CoV through three key residues in RBD

To understand the reason for why CC12.1 could bind with SARS-CoV-2 specifically but not with SARS-CoV, we carried out MD simulation with SARS-CoV RBD-ACE2 complex (PDB ID: 2AJF) (Fig. 6A). In the following text, we use SARS-CoV-2 sequence number to compare with the corresponding number for SARS-CoV with a subscript "S1." Conserved interactions were found for SARS-CoV and SARS-CoV-2 due to the high similarity of sequences, including hydrogen bonds formed by $Y436_{S1}$-D30, $N479_{S1}$-K31, $Y491_{S1}$-E37, $N473_{S1}$-Y83, $G488_{S1}$-K353 and $T486_{S1}$-D355. The occurrence of the last two hydrogen bonds achieved as high as 98.73% and 90.58%, respectively (Fig. 6B and C, Table S2). Besides, hydrophobic contacts still form among $L472_{S1}$, L79 and M82, although F486 of SARS-CoV-2 RBD mutates to $L472_{S1}$ in SARS-CoV. Special attention has been paid on those crucial residues for SARS-CoV-2 antibody/ ACE2 binding but not dedicated to efficient SARS-CoV ACE2 binding. Due to the K417 → $V404_{S1}$ mutation, D30 of ACE2 forms
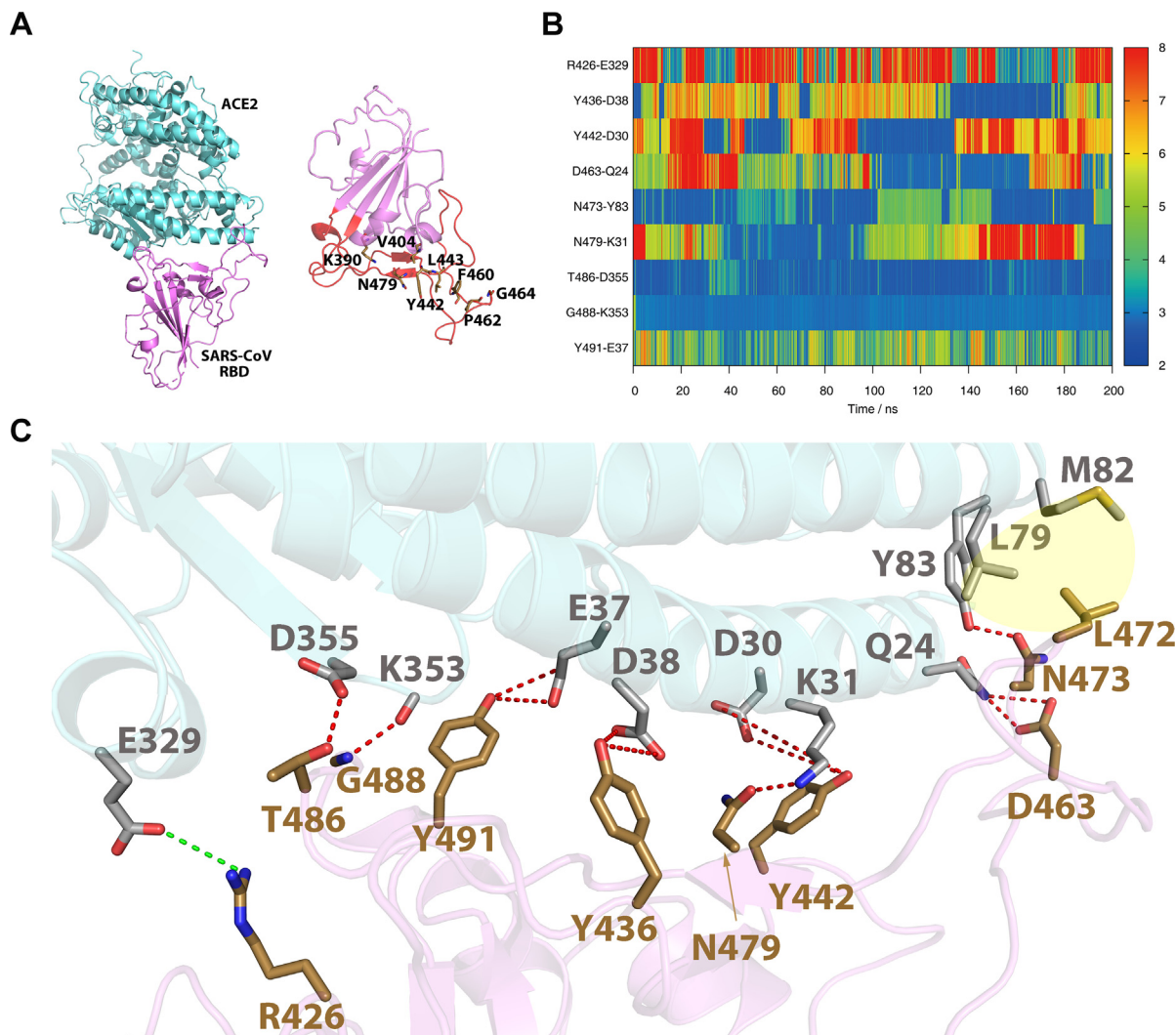

Fig. 6. Crystal structure of SARS-CoV RBD-ACE2 complex and represented interactions between SARS-CoV RBD and ACE2. (A) The RBD and ACE2 structures are displayed in cartoon, colored in violet and aquamarine respectively (Left). The receptor binding motif (RBD) of the SARS-CoV RBD is colored in red, and the key mutated residues in RBDs are labeled and shown in sticks (Right). (B) Distances between each pair of residues forming hydrogen bond and salt bridge in ACE2 bound complex during the 200 ns simulations. (C) Interactions between the SARS-CoV RBD and ACE2. Key residues of the SARS-CoV RBD, ACE2 are shown as sticks with carbon atoms colored in brown, gray, respectively. Hydrogen bonds and salt bridges are displayed in red and green dash lines, respectively. Hydrophobic interactions are shaded in yellow background. (For interpretation of the references to colour in this figure legend, the reader is referred to the web version of this article.)

a fluctuant hydrogen bond with Y442 for only 32.61% of simulation in SARS-CoV RBD-ACE2 complex instead of forming the salt bridge with K417 of SARS-CoV-2 RBD.

Previous study reported the importance of V404$_{S1}$ → K417 mutation for enhancing the ACE2 binding of SARS-CoV-2 RBD [25]. To evaluate the impact of this mutation on antibody binding to SARS-CoV-2 RBD, single mutation from K417 to V has been established and results in obvious perturbation to binding affinity by increasing binding free energy of 7.41 ± 0.94 kcal/mol (Table 1). In addition, some escape mutations locate in the distal motif and cause the neutralization failure of some mAbs that share the same recognition region with CC12.1 [41]. Since residues on distal motif contribute specific interaction in SARS-CoV-2 RBD-antibody complex and the limited conversation of the distal motif region, further single mutations were also implemented. The Y473 → F460$_{S1}$ mutation may directly lead to the break of Y473-V$_H$ S31 interaction because of the phenolic hydroxyl group deletion. The A475 → P462$_{S1}$ displacement may cause conformation change against with CC12.1 binding, due to the increased rigidity caused by Pro residue [25]. S477 was found to be the most frequent mutated residue on distal motif. Thus, these three residue mutations were simulated for binding free energy calculation (Fig. S7B). Results show increasing energy value of 1.06 ± 1.09 kcal/mol and 5.26 ± 0.99 kcal/mol for Y473 → F460$_{S1}$ and A475 → P462$_{S1}$, respectively. However, S477 → G464 mutation increases binding affinity by −2.92 ± 0.98 kcal/mol, perhaps due to the reduction of electrostatic repulsion with V$_L$ G26 of CC12.1. Finally, K417, Y473 and A475 were identified as key residues dedicating to binding specificity of SARS-CoV-2 antibody.

Our results show that mutations of several key residues may cause the loss of antibody cross-neutralization between SARS-CoV-2 and SARS-CoV, which may explain why only limited cross-neutralization activity was found in convalescent sera obtained from SARS-CoV and SARS-CoV-2 patients [15]. Several reinfection cases have been reported and the whole genome analysis shows the differences between the SARS-CoV-2 strains from the first and second episode [42–44]. This indicates that none of only one type of antibody would perfectly protect people from infection. To resist the potential mutational escape of different SARS-CoV-2 strains, the antibody cocktail therapy could be used [45,46]. One of the dilemmas of the cocktail therapy is how to confirm the composition of antibodies accurately and efficiently. The mutation sites in virus can be obtained by sequencing the virus genome and what kind of antibody might show neutralization activity towards to SARS-CoV-2 can be determined through our results. To a certain extent, key residues identified for antibody specificity and the importance of distal motif revealed may reflect the structural basis of IGHV3-53 encoded antibodies response to SARS-CoV-2, promoting the antibody design and inspiring the composition of antibody cocktail therapy.

3. Conclusion

Neutralization towards to the severe acute respiratory syndrome coronavirus 2 (SARS-CoV-2) by antibody is one of the most efficient therapies to against infection. Through MD simulations, the distal motif (residue numbers 473–488) of RBD which shares electrostatic complementarity with SARS-CoV-2 RBD and greatly stabilizes the conformation of SARS-CoV-2 RBD with antibody bound was identified. The distal motif is very unstable with ACE2 bound because of the unstable and narrow hydrogen-bonding network formed between these two proteins, which indicates the difference between the binding modes of antibody binding and receptor binding. Key epitopes, including D405, K417, Y421, Y453, L455, R457, Y473, A475, N487, G502 and Y505, dedicating

to efficient antibody binding were revealed. Two conserved motifs, SNY and SGGS in CC12.1 antibody that interact with key epitopes efficiently were identified. By forming extensive and stable hydrogen-bonding networks, enhanced binding competitivity of antibody has been achieved compared to receptor ACE2. Two single site mutations, V$_H$ V98E and V$_L$ G68D in antibody are proposed to imitate the interactions between SARS-CoV-2 RBD and the receptor. These two single site mutations could enhance antibody binding which was validated by relative free energies calculation and molecular docking. Three residues, K417, Y473 and A475 are found crucial for specific binding of SARS-CoV-2 rather than SARS-CoV by antibody. Our study illustrates essential information for not only efficiency but also specificity of SARS-CoV-2 antibody on structural basis to promote advanced antibody design.

4. Experimental

4.1. Structure analysis of crystal structures

Crystal structures of three complexes, PDB ID: 6XC2, which includes SARS-CoV-2 RBD and CC12.1 antibody [29]; PDB ID: 6M17, which includes the SARS-CoV-2 RBD and the human ACE2 [38]; PDB ID: 2AJF [21], which includes the SARS-CoV RBD and the human ACE2, were visualized and generated surface views using PyMOL program [47]. The hydrogen atoms were added by PDB2PQR webserver [48], and the electrostatic potentials were calculated using Adaptive Poisson-Boltzmann Solver (APBS) [49] in PyMOL. Multiple sequence alignment were created using Clustal W [50], and the results were mapped using ESPript webserver [51]. GenBank accession numbers are: MN908947.1 for SARS-CoV-2 Spike; NC_004718.3 for SARS-CoV Spike; KY417151.1 for Bat_SL_Rs7327 Spike; KY417150.1 for Bat_SL_Rs4874 Spike; KY417146.1 for Bat_SL_Rs4231 Spike.

4.2. Molecular dynamics simulations

The crystal structures of complexes between SARS-CoV-2 RBD and CC12.1 antibody (PDB ID: 6XC2) and complexes between the RBD and human ACE2 (PDB ID: 6M17 and PDB ID: 2AJF) were used as the starting structure for MD simulations. Apo protein of SARS-CoV-2 RBD was extracted from the crystal structure of PDB ID: 6M17. The protonation states of proteins were investigated and modified using the H++ webserver [52]. All proteins were applied with Amber ff14SB force field for the protein [53,54] and solvated in a rectangular box of TIP3P water [55], with a minimum distance between the protein and the box edge of 8 Å. The solvated protein was subsequently neutralized with Na$^+$ ion or Cl$^-$ ion. Optimization and equilibration were applied to all systems before running production MD simulation. Initial optimization of the solvent consisted of 1000 cycles of energy minimization was followed by 50 ps of MD simulation at 298 K (applying a positional restraint of 10 kcal mol^{-1} Å^{-2} on all solute atoms). The whole system was then optimized by 1000 cycles of energy minimization with a restraint on the protein Cα atoms (2.0 mol^{-1} Å^{-2}). To prepare for production simulations, first, the temperature was increased from 50 to 298 K over a period of 10 ps (maintaining the mild restraint on Cα atoms). Second, 50 ps simulation in the NPT ensemble at 298 K and a pressure of 1 bar was performed, again maintaining the mild restraint on Cα atoms. Thereafter, the whole system was briefly further equilibrated by 100 ps of NPT MD simulation (298 K, 1 bar). After this equilibration procedure, 200 ns MD simulation in the NPT ensemble at 298 K and 1 bar was carried out. Throughout, periodic boundary conditions were applied and the SHAKE algorithm was applied to fix all bond lengths involving hydrogen atoms. A time step of 2 fs was used, with a direct-space cut off

radius of 8.0 Å for non-bonded interactions and particle mesh Ewald for long-range electrostatic interactions. The trajectory was sampled every 1 ps (500 steps intervals) for analysis. All simulations were performed using AMBER18 program [53].

4.3. Analysis of MD simulations

The AmberTools programs cpptraj [56] and MMGBSA [57] were used for analyzing trajectories. Structures were visualized using VMD [58]. The RMSD and RMSF values of the systems were calculated after imaging on the structure of the 200 ns trajectory. Distances of hydrogen-bonding (distance cut-off of 3.50 Å), salt bridge (distance cut-off of 4.00 Å) and hydrophobic interaction (distance cut-off of 4.60 Å) were computed using WORDOM [59], and mapped as heat map using GNUPLOT [60]. The information of SARS-CoV-2 genomic epidemiology was obtained from GISAID database [33]. To calculate the relative binding free energies ($\Delta\Delta G$) caused by residue mutations, residue name was changed manually in crystal structure (PDB ID: 6XC2) and side chain deleted previously was modified using tleap. Exactly the same optimization and equilibration protocols were used for MD simulations of the modified crystal structures. In the following, production simulation of 5 ns was performed. MMGBSA was used to calculate the binding free energies of mutated complexes, and the calculated results were compared with the binding energy of the first 5 ns simulation of SARS-CoV-2 RBD-CC12.1 complex (PDB ID: 6XC2) to get the relative free energies of binding $\Delta\Delta G$.

4.4. Molecular docking

All the docking experiments were conducted by HDOCK webserver [61,62]. Crystal structures of human CD147 and SARS-CoV-2 RBD were obtained from PDB ID: 3B5H, chain B and PDB ID: 6M17, chain E respectively. The mutated CC12.1 structure that used for docking was extracted from the first frame of 5 ns production simulation to avoid the potential conformation bump. The crystal structures of SARS-CoV-2 RBD that used for docking on mutated CC12.1 was obtain form PDB ID: 6XC2, chain Z.

Finally, all the materials and methods we used were shown as a workflow (Fig. S9).

CRediT authorship contribution statement

Daojiong Wang: Conceptualization, Validation, Formal analysis, Investigation, Writing - original draft. **Yushu Ge:** Conceptualization, Validation, Formal analysis, Article review. **Bin Zhong:** Formal analysis, Investigation. **Dan Liu:** Supervision.

Declaration of Competing Interest

The authors declare that they have no known competing financial interests or personal relationships that could have appeared to influence the work reported in this paper.

Acknowledgments

Appendix A. Supplementary data

Supplementary data to this article can be found online at https://doi.org/10.1016/j.csbj.2021.03.021.

References

[1] Wu F, Zhao S, Yu B, Chen YM, Wang W, et al. A new coronavirus associated with human respiratory disease in China. Nature 2020;579:265–9.

[2] Drosten C, Günther S, Preiser W, van der Werf S, Brodt H-R, Becker S, et al. Identification of a novel coronavirus in patients with severe acute respiratory syndrome. New Engl J Med 2003;348:1967–76.

[3] Sohrabi C, Alsafi Z, O'Neill N, Khan M, Kerwan A, Al-Jabir A, et al. World Health Organization declares global emergency: A review of the 2019 novel coronavirus (COVID-19). Int J Surg 2020;76:71–6.

[4] World Health Organization (2021) Weekly operational update on COVID-19 – 22 February 2021. Available: https://www.who.int/publications/m/item/weekly-operational-update-on COVID-19—22-february-2021. Accessed 2021 Feb 23.

[5] Cao B, Wang Y, Wen D, Liu W, Wang J, Fan G, et al. A trial of lopinavir-ritonavir in adults hospitalized with severe COVID-19. New Engl J Med 2020;382:1787–99.

[6] Borba MGS, Val FFA, Sampaio VS, Alexandre MAA, Melo GC, et al. Effect of high vs low doses of chloroquine diphosphate as adjunctive therapy for patients hospitalized with severe acute respiratory syndrome coronavirus 2 (SARS-CoV-2) infection a randomized clinical trial. Jama Netw Open 2020;3:e208857.

[7] Wang Y, Zhang D, Du G, Du R, Zhao J, Jin Y, et al. Remdesivir in adults with severe COVID-19: a randomised, double-blind, placebo-controlled, multicentre trial. Lancet 2020;395:1569–78.

[8] Consortium WHOST, Pan H, Peto R, Henao-Restrepo AM, Preziosi MP, et al. (2021) Repurposed Antiviral Drugs for COVID-19 - Interim WHO Solidarity Trial Results. N Engl J Med 384: 497-511.

[9] Tay MZ, Poh CM, Rénia L, MacAry PA, Ng LFP. The trinity of COVID-19: immunity, inflammation and intervention. Nat Rev Immunol 2020;20:363–74.

[10] Amanat F, Krammer F. SARS-CoV-2 Vaccines: Status Report. Immunity 2020;52:583–9.

[11] Lurie N, Saville M, Hatchett R, Halton J. Developing COVID-19 vaccines at pandemic speed. New Engl J Med 2020;382:1969–73.

[12] Su S, Du L, Jiang S. Learning from the past: development of safe and effective COVID-19 vaccines. Nat Rev Microbiol 2021;19(3):211–9.

[13] Zhao J, Zhao S, Ou J, Zhang J, Lan W, Guan W, et al. COVID-19: Coronavirus Vaccine Development Updates. Front Immunol 2020;11:602256.

[14] Voysey M, Clemens SAC, Madhi SA. Safety and efficacy of the mAb nCoV-19 vaccine (AZD1222) against SARS-CoV-2: an interim analysis of four randomised controlled trials in Brazil, South Africa, and the UK. Lancet 2021;397:99–111.

[15] Ou X, Liu Y, Lei X, Li P, Mi D, Ren L, et al. Characterization of spike glycoprotein of SARS-CoV-2 on virus entry and its immune cross-reactivity with SARS-CoV. Nat Commun 2020;11(1):1620.

[16] Bhattacharya M, Sharma AR, Mallick B, Sharma G, Lee S-S, Chakraborty C. Immunoinformatics approach to understand molecular interaction between multi-epitopic regions of SARS-CoV-2 spike-protein with TLR4/MD-2 complex. Infect Genet Evol 2020;85:104587.

[17] Tai W, He L, Zhang X, Pu J, Voronin D, Jiang S, et al. Characterization of the receptor-binding domain (RBD) of 2019 novel coronavirus: implication for development of RBD protein as a viral attachment inhibitor and vaccine. Cell Mol Immunol 2020;17:613–20.

[18] Rogers TF, Zhao F, Huang D, Beutler N, Burns A, He W-T, et al. Isolation of potent SARS-CoV-2 neutralizing antibodies and protection from disease in a small animal model. Science 2020;369:956–63.

[19] Walls AC, Park Y-J, Tortorici MA, Wall A, McGuire AT, Veesler D. Structure, Function, and Antigenicity of the SARS-CoV-2 Spike Glycoprotein. Cell 2020;181:281–92.

[20] Hoffmann M, Kleine-Weber H, Schroeder S, Krüger N, Herrler T, Erichsen S, et al. SARS-CoV-2 cell entry depends on ACE2 and TMPRSS2 and is blocked by a clinically proven protease inhibitor. Cell 2020;181:271–80.

[21] Li F, Li WH, Farzan M, Harrison SC. Structure of SARS coronavirus spike receptor-binding domain complexed with receptor. Science 2005;309:1864–8.

[22] Li W, Moore MJ, Vasilieva N, Sui J, Wong SK, Berne MA, et al. Angiotensin-converting enzyme 2 is a functional receptor for the SARS coronavirus. Nature 2003;426:450–4.

[23] Lan J, Ge J, Yu J, Shan S, Zhou H, Fan S, et al. Structure of the SARS-CoV-2 spike receptor-binding domain bound to the ACE2 receptor. Nature 2020;581:215–20.

[24] Wrapp D, Wang N, Corbett KS, Goldsmith JA, Hsieh C-L, Abiona O, et al. Cryo-EM structure of the 2019-nCoV spike in the prefusion conformation. Science 2020;367:1260–3.

[25] Wang YJ, Liu MY, Gao JL. Enhanced receptor binding of SARS-CoV-2 through networks of hydrogen-bonding and interactions. Proc Natl Acad Sci U S A 2020;117:13967–74.

[26] Tian X, Li C, Huang A, Xia S, Lu S, Shi Z, et al. Potent binding of 2019 novel coronavirus spike protein by a SARS coronavirus-specific human monoclonal antibody. Emerg Microbes Infect 2020;9:382–5.

[27] Wang Z, Schmidt F, Weisblum Y, Muecksch F, Barnes CO, et al. (2021) mRNA vaccine-elicited antibodies to SARS-CoV-2 and circulating variants. Nature. https://doi.org/10.1038/s41586-021-03324-6.

[28] Kemp SA, Collier DA, Datir RP, Ferreira I, Gayed S, et al. (2021) SARS-CoV-2 evolution during treatment of chronic infection. Nature. https://doi.org/10.1038/s41586-021-03291-y.

[29] Yuan M, Liu H, Wu NC, Lee C-C, Zhu X, Zhao F, et al. Structural basis of a shared antibody response to SARS-CoV-2. Science 2020;369:1119–23.

[30] Ulrich H, Pillat MM. CD147 as a target for COVID-19 treatment: suggested effects of azithromycin and stem cell engagement. Stem Cell Rev Rep 2020;16:434–40.

[31] Shang J, Ye G, Shi K, Wan Y, Luo C, Aihara H, et al. Structural basis of receptor recognition by SARS-CoV-2. Nature 2020;581:221–4.

[32] Hu B, Zeng LP, Yang XL, Ge XY, Zhang W, et al. (2017) Discovery of a rich gene pool of bat SARS-related coronaviruses provides new insights into the origin of SARS coronavirus. Plos Path 13: e1006698.

[33] Elbe S, Buckland-Merrett G. Data, disease and diplomacy: GISAID's innovative contribution to global health. Glob Chall 2017;1:33–46.

[34] Li L, Sun T, He YF, Li WD, Fan YB, et al. Epitope-based peptide vaccines predicted against novel coronavirus disease caused by SARS-CoV-2. Virus Res 2020;288:198082.

[35] Greaney AJ, Starr TN, Gilchuk P, Zost SJ, Binshtein E, Loes AN, et al. Complete mapping of mutations to the SARS-CoV-2 spike receptor-binding domain that escape antibody recognition. Cell Host Microbe 2021;29(1):44–57.

[36] Veeramachaneni GK, Thunuguntla VB, Bobbillapati J, Bondili JS. Structural and simulation analysis of hotspot residues interactions of SARS-CoV 2 with human ACE2 receptor. J Biomol Struct Dyn 2020. https://doi.org/10.1080/07391102.2020.1773318.

[37] Starr TN, Greaney AJ, Hilton SK, Ellis D, Crawford KHD, Dingens AS, et al. Deep mutational scanning of SARS-CoV-2 receptor binding domain reveals constraints on folding and ACE2 binding. Cell 2020;182:1295–310.

[38] Yan R, Zhang Y, Li Y, Xia Lu, Guo Y, Zhou Q. Structural basis for the recognition of SARS-CoV-2 by full-length human ACE2. Science 2020;367:1444–8.

[39] Mukherjee S, Tworowski D, Detroja R, Mukherjee SB, Frenkel-Morgenstern M. Immunoinformatics and structural analysis for identification of immunodominant epitopes in SARS-CoV-2 as potential vaccine targets. Vaccines 2020;8:290.

[40] Waman VP, Sen N, Varadi M, Daina A, Wodak SJ, et al. (2020) The impact of structural bioinformatics tools and resources on SARS-CoV-2 research and therapeutic strategies. Brief Bioinform https://doi.org/10.1093/bib/bbaa362.

[41] Liu Z, VanBlargan LA, Bloyet L-M, Rothlauf PW, Chen RE, Stumpf S, et al. Identification of SARS-CoV-2 spike mutations that attenuate monoclonal and serum antibody neutralization. Cell Host Microbe 2021;29:477–88.

[42] To KK, Hung IF, Ip JD, Chu AW, Chan WM, et al. COVID-19 re-infection by a phylogenetically distinct SARS-coronavirus-2 strain confirmed by whole genome sequencing. Clin Infect Dis 2020. https://doi.org/10.1093/cid/ciaa1275.

[43] Tillett RL, Sevinsky JR, Hartley PD, Kerwin H, Crawford N, Gorzalski A, et al. Genomic evidence for reinfection with SARS-CoV-2: a case study. Lancet Infect Dis 2021;21:52–8.

[44] Gupta V, Bhoyar RC, Jain A, Srivastava S, Upadhayay R, et al. Asymptomatic reinfection in two healthcare workers from India with genetically distinct SARS-CoV-2. Clin Infect Dis 2020. https://doi.org/10.1093/cid/ciaa1451.

[45] Hansen J, Baum A, Pascal KE, Russo V, Giordano S, Wloga E, et al. Studies in humanized mice and convalescent humans yield a SARS-CoV-2 antibody cocktail. Science 2020;369:1010–4.

[46] Baum A, Fulton BO, Wloga E, Copin R, Pascal KE, Russo V, et al. Antibody cocktail to SARS-CoV-2 spike protein prevents rapid mutational escape seen with individual antibodies. Science 2020;369:1014–8.

[47] Schrodinger, LLC. The PyMOL Molecular Graphics System, Version 2.4; 2020.

[48] Dolinsky TJ, Nielsen JE, McCammon JA, Baker NA. PDB2PQR: an automated pipeline for the setup of Poisson-Boltzmann electrostatics calculations. Nucleic Acids Res 2004;32:W665–7.

[49] Baker NA, Sept D, Joseph S, Holst MJ, McCammon JA. Electrostatics of nanosystems: application to microtubules and the ribosome. Proc Natl Acad Sci U S A 2001;98:10037–41.

[50] Larkin MA, Blackshields G, Brown NP, Chenna R, McGettigan PA, McWilliam H, et al. Clustal W and clustal X version 2.0. Bioinformatics 2007;23:2947–8.

[51] Robert X, Gouet P. Deciphering key features in protein structures with the new ENDscript server. Nucleic Acids Res 2014;42:W320–4.

[52] Anandakrishnan R, Aguilar B, Onufriev AV. H++3.0: automating pK prediction and the preparation of biomolecular structures for atomistic molecular modeling and simulations. Nucleic Acids Res 2012;40:W537–41.

[53] Case IYB-S DA, Brozell SR, Cerutti CZ, Cheatham TE, III, V.W.D. Cruzeiro, et al. (2019) AMBER 2019. San Francisco: University of California. 960p.

[54] Salomon-Ferrer R, Case DA, Walker RC. An overview of the Amber biomolecular simulation package. Wiley Interdiscip Rev Comput Mol Sci 2013;3:198–210.

[55] Jorgensen WL, Chandrasekhar J, Madura JD, Impey RW, Klein ML. Comparison of simple potential functions for simulating liquid water. J Chem Phys 1983;79:926–35.

[56] Roe DR, Cheatham TE. PTRAJ and CPPTRAJ: software for processing and analysis of molecular dynamics trajectory data. J Chem Theory Comput 2013;9:3084–95.

[57] Miller BR, McGee TD, Swails JM, Homeyer N, Gohlke H, et al. MMPBSA.py: an efficient program for end-state free energy calculations. J Chem Theory Comput 2012;8:3314–21.

[58] Humphrey W, Dalke A, Schulten K. VMD: Visual molecular dynamics. J Mol Graph 1996;14:33–8.

[59] Seeber M, Cecchini M, Rao F, Settanni G, Caflisch A. Wordom: a program for efficient analysis of molecular dynamics simulations. Bioinformatics 2007;23:2625–7.

[60] Racine J. gnuplot 4.0: A portable interactive plotting utility. J Appl Economet 2006;21:133–41.

[61] Yan YM, Zhang D, Zhou P, Li BT, Huang SY. HDOCK: a web server for protein-protein and protein-DNA/RNA docking based on a hybrid strategy. Nucleic Acids Res 2017;45:W365–73.

[62] Yan YM, Tao HY, He JH, Huang SY. The HDOCK server for integrated protein-protein docking. Nat Protoc 2020;15:1829–52.